Solitons in Bragg gratings with saturable nonlinearities

Ilya M. Merhasin,[1] Boris A. Malomed,[1] K. Senthilnathan,[2,*] K. Nakkeeran,[3] P. K. A. Wai,[2] and K. W. Chow[4]

[1]*Department of Interdisciplinary Studies, School of Electrical Engineering, Faculty of Engineering, Tel Aviv University, Tel Aviv 69978, Israel*
[2]*Photonics Research Center and Department of Electronic and Information Engineering, The Hong Kong Polytechnic University, Hung Hom, Kowloon, Hong Kong*
[3]*Department of Engineering, Fraser Noble Building, King's College, University of Aberdeen, Aberdeen AB24 3UE, UK*
[4]*Department of Mechanical Engineering, University of Hong Kong, Pokfulam Road, Hong Kong*
[*]*Corresponding author: ensenthe@polyu.edu.hk*

Received December 8, 2006; revised February 6, 2007; accepted February 27, 2007; posted March 23, 2007 (Doc. ID 77804); published June 15, 2007

We introduce two different systems of coupled-mode equations to describe the interaction of two waves coupled by the Bragg reflection in the presence of saturable nonlinearity. The basic model assumes the ordinary linear coupling between the modes. It may be realized as a photorefractive waveguide, with a Bragg lattice permanently written in its cladding. We demonstrate the presence of a cutoff point in the system's bandgap, with gap solitons existing only on one side of it. Close to this point, the soliton's norm diverges with power −3/2. The soliton family between the cutoff point and the edge of the bandgap is stable. In this model, stationary bound states of two in-phase solitons are found too, but they are unstable, transforming themselves into breathers. Another model assumes a photoinduced longitudinal bulk grating, with the corresponding intermode coupling subject to saturation along with the nonlinearity. In that model, another cutoff point is found, with the soliton's norm diverging near it with power −2. Solitons are stable in this model too (while it does not give rise to two-soliton bound states). Collisions between moving solitons are always quasi-elastic, in either model. © 2007 Optical Society of America

OCIS codes: 060.5530, 190.5530, 350.2770.

1. INTRODUCTION AND THE MODELS

Periodic structures in optical waveguides known as Bragg gratings (BGs), which provide for resonant reflection of light, and thus strong linear coupling between counterpropagating waves, have been a subject of intensive theoretical and experimental research, due to their numerous applications to optical sensors and various telecommunication devices (such as add–drop multiplexers, dispersion compensators, narrowband filters, etc. [1]), as well as their great potential as media for fundamental studies of nonlinear optical dynamics [2]. A notable feature of these periodic structures is the presence of the stopband, alias photonic bandgap, in the linear spectrum. The combination of the bandgap (that generates extremely strong effective dispersion in the temporal domain, or effective diffraction in the spatial-domain realization of the BG, near edges of the bandgap) with the waveguide's material nonlinearity gives rise to a variety of effects, such as optical bistability, limiting, and modulational instability. An especially interesting manifestation of the nonlinearity is the formation of BG solitons (alias gap solitons, if they are spectrally centered inside the bandgap). A standard theoretical model of a Kerr-nonlinear medium equipped with the BG is based on a system of coupled-mode equations (CMEs) for amplitudes of the counterpropagating waves, $U(x,t)$ and $V(x,t)$, which are coupled linearly by the BG reflection, and nonlinearly by the cross-phase modulation (XPM), and also take into account the self-phase modulation (SPM) effect [3]:

$$iU_t + iU_x + (\sigma|U|^2 + |V|^2)U + \kappa V = 0,$$

$$iV_t - iV_x + (\sigma|V|^2 + |U|^2)V + \kappa U = 0, \tag{1}$$

where, in the most relevant case of the BG in the optical fiber, x and t are the coordinates along the fiber and time, and κ is the Bragg reflectivity (i.e., the coefficient of the intermode linear coupling), while the group velocity of light and the overall Kerr coefficient are scaled to be 1. The value of the SPM to XPM ratio in Eqs. (1) corresponding to the ordinary Kerr nonlinearity is $\sigma=1/2$.

Within the framework of Eqs. (1), a family of exact soliton solutions is available (for any value of σ), with two intrinsic parameters, which determine the soliton's amplitude and velocity [4,5]. The stability of these solutions was first studied by means of the variational approximation [6], and then with the help of accurate numerical methods [7,8]. It was found that approximately half of the gap-soliton family is stable, and the other half unstable (the solitons with positive and negative intrinsic frequencies are, respectively, stable and unstable). Moving BG solitons (with the velocity no less than half the group ve-

locity of light in the same material) have been created experimentally in silica fibers with the BG written in the cladding [9,10].

In addition to the studies of temporal gap solitons in fiber BGs, much effort has been focused on gap solitons in the spatial domain, which were predicted in Refs. [11,12] and later theoretically elaborated in detail in various settings [13–16]. In particular, Eqs. (1), with t and x realized, respectively, as the propagation distance and transverse coordinate, provide for a model of the copropagation of two waves in a nonlinear planar waveguide, the waves being linearly coupled by the Bragg reflection from a longitudinal lattice of parallel riblets or grooves on the waveguide's surface ("longitudinal" means that the grating is drawn parallel to the propagation axis, whereas the Poynting vectors of the two waves make angles $\pm\theta$ with the axis; see Eqs. (9) below]. In the experiment, one-dimensional (1D) spatial gap solitons were created in quasi-discrete waveguide arrays with the Kerr nonlinearity [17–19], as well as in arrays of photovoltaic waveguides in $LiNbO_3$ [20]. Parallel to that, 1D [21,22] and two-dimensional (2D) [23] spatial solitons of the gap-type were created in photonic lattices, which can be optically induced in photorefractive media (that feature saturable, rather than cubic, nonlinearity), using the technique proposed in [24,25] and then applied to the creation of spatial solitons of various types; see review [26].

The recent experimental demonstration of discrete radial solitons in an axially symmetric photonic lattice induced in a photorefractive material [27] suggests that gap solitons may be created in that setting too, as recently shown in detail in a 2D model with the cubic nonlinearity [28] (for the first time, solitons in a radial potential combined with the cubic nonlinearity were considered in [29,30]). However, in the present work, we only deal with 1D models.

The objective of the present work is to propose physically relevant systems of CMEs with saturable nonlinearity, modeling BGs in photorefractive media, and find families of gap-soliton solutions in those systems (including the investigation of the soliton stability). The evolution of local amplitude $E(x,z)$ of the electromagnetic field along the propagation coordinate z in a photorefractive material equipped with the photonic lattice, of period $2\pi/K$ and strength I_0, is described by the well-known equation [24,25]. In the normalized form, it is

$$i\frac{\partial E}{\partial z}+\frac{1}{2}\frac{\partial^2 E}{\partial x^2}-\frac{E}{1+I_0\cos^2(Kx)+|E|^2}=0, \tag{2}$$

where x is the transverse coordinate. A natural issue is to derive CMEs from Eq. (2), substituting the field as a superposition of two waves coupled by the Bragg reflection, $E(x,z)=U(x,z)e^{iKx}+V(x,z)e^{-iKx}$, where the amplitudes U and V are assumed to be slowly varying functions of x in comparison with the carrier waves, $\exp(\pm iKx)$. The derivation was performed in [31], by expanding the nonlinear term in Eq. (2) into a Fourier series and keeping the lowest-order harmonics. The result is a system of CMEs with a specific form of saturable nonlinearity, which implicitly contains four-wave mixing, along with SPM and XPM:

$$i\frac{\partial U}{\partial z}+iK\frac{\partial U}{\partial x}=\frac{(U-V)}{\sqrt{1+I_0(1+|U-V|^2)+2(|U|^2+|V|^2)}},$$

$$i\frac{\partial V}{\partial z}-iK\frac{\partial V}{\partial x}=\frac{(V-U)}{\sqrt{1+I_0(1+|U-V|^2)+2(|U|^2+|V|^2)}}. \tag{3}$$

CMEs were derived in [31] also for a 2D configuration, when the angles between the wave vectors carrying the field amplitudes U and V and the propagation axis (z) are different from 90°. In the latter case, the equations feature a different saturable nonlinearity,

$$i\frac{\partial U}{\partial z}+iK\frac{\partial U}{\partial x}=\frac{(U-V)}{\sqrt{I_0(1+|U|^2+|V|^2)}},$$

$$i\frac{\partial V}{\partial z}-iK\frac{\partial V}{\partial x}=\frac{(V-U)}{\sqrt{I_0(1+|U|^2+|V|^2)}} \tag{4}$$

[rescaling x, one may set $K=1$ in Eqs. (3) and (4), and constant I_0, which is an irreducible parameter in Eqs. (3), can be scaled out from Eqs. (4); hence the latter equations do not contain any irreducible coefficient]. Note that Eqs. (4), unlike Eqs. (3), feature solely SPM and XPM effects, without four-wave mixing. It is noteworthy too that both systems, Eqs. (3) and (4), demonstrate not only the saturation of the SPM and XPM terms in each equation, but also the saturation of the coupling between the two waves [the coupling is no longer purely linear; cf. Eqs. (1)].

Gap-soliton solutions (including *tilted* ones, i.e., counterparts of moving solitons in the temporal domain) to Eqs. (3) and (4) were found in [31], and their stability was investigated by means of direct simulations. Nontrivial internal stability borders in the soliton families were found [in particular, two disjoint stability areas were discovered in the model based on Eqs. (4)].

These results, as well as more general arguments, suggest studying BG solitons in physically relevant systems with the most fundamental saturable nonlinearity, which resembles that in Eqs. (4), but is rational, rather than algebraic. We introduce two models, one of which combines the saturable nonlinearity and ordinary linear intermode coupling, and another, more formal one (see an explanation of the physical realization of the models below), in which the coupling between the two waves is also subject to the saturation. The former model is based on the following CMEs in a normalized form; cf. Eqs. (1) and (4),

$$iU_t+iU_x-\frac{U}{1+|U|^2+|V|^2}+\kappa V=0,$$

$$iV_t-iV_x-\frac{V}{1+|U|^2+|V|^2}+\kappa U=0. \tag{5}$$

The latter model (also cast in the normalized form) is more similar to Eqs. (4):

$$iU_t + iU_x - \frac{U - \kappa V}{1 + |U|^2 + |V|^2} = 0,$$

$$iV_t - iV_x - \frac{V - \kappa U}{1 + |U|^2 + |V|^2} = 0. \quad (6)$$

In either system, Eqs. (5) or (6), we assume that U and V are amplitudes of two independent waves, with the total intensity of light approximated by $|U|^2+|V|^2$, as commonly adopted in various settings [26,32–34]. This is a difference from the BG model in the Kerr medium, based on Eqs. (1), where the relevant combination of the nonlinear terms has $\sigma=1/2$ [nevertheless, exact soliton solutions of Eqs. (1) are available for any σ [4], including $\sigma=1$, which corresponds to combination $|U|^2+|V|^2$]. Note also that, unlike Eqs. (1), the coupling constant κ (which is proportional to the Bragg reflectivity of the corresponding grating) cannot be scaled out (set equal to 1) in Eqs. (5) and (6).

The dispersion relation of the linearized version of Eqs. (5) or (6), obtained by the substitution of $U,V \sim e^{iqx-i\omega t}$ (with arbitrary wavenumber q), coincides with that of Eqs. (1), except for the frequency offset by $\Delta\omega=1$,

$$\omega = 1 \pm \sqrt{\kappa^2 + q^2} \quad (7)$$

[in fact, the choice of $\Delta\omega=1$ fixes the normalization adopted in Eqs. (5) and (6)]. As follows from Eq. (7), the bandgap in the linear spectrum of either model is

$$1 - \kappa < \omega < 1 + \kappa \quad (8)$$

(by definition, we set $\kappa>0$).

Proceeding to physical realization of the models introduced above, the coupled-mode equations (5) can be implemented in a straightforward way if one assumes a planar waveguide, based on a slab of a photorefractive material (without any built-in lattice), which is sandwiched between two cladding layers (made of an ordinary optical material). Each layer carries a permanent longitudinal BG, i.e., one written (on the layer) parallel to the propagation direction. Since the objective is to predict spatial solitons in this setting [hence t in Eqs. (5) is to be realized as the propagation distance and x as the transverse coordinate in the plane of the waveguide], the medium can be described by 1D equations if the thickness of the photorefractive layer, $d_\perp$, is smaller than a typical transverse width, $W_\perp$, of the 2D spatial soliton in photorefractive crystals. As predicted in theoretical analysis [35], and confirmed by experimental observations in nearly isotropic, [strontium barium niobate (SBN)] [36] and strongly anisotropic ($KNbO_3$) [37] crystals, the soliton-forming beam with the power in the microwatt range gives rise to spatial solitons with $W_\perp$ taking values in the range of 10–30 μm. Thus, the 1D approximation may be well justified for $d_\perp \lesssim 10\ \mu$m. If the thickness of the cladding layers, in which the grating is written, is $\simeq 2\ \mu$m (a natural size of the cladding), the effective strength of the grating (i.e., the Bragg reflectivity), averaged in the transverse direction, will be ~50% of its actual strength in the cladding. The latter characteristic may be defined as the inverse reflection length; usually, it is $1/l_{\rm refl}^{\rm (Bragg)} \sim 1\ {\rm mm}^{-1}$, for weak gratings [1]. Since the propagation length necessary for the formation and detection of gap solitons amounts to several $l_{\rm refl}^{\rm (Bragg)}$ [3], the typical longitudinal size of available waveguides, several centimeters, will be quite sufficient for experiments with the spatial BG solitons in this setting.

Note that Eqs. (5) and (6) neglect the bulk diffraction. To estimate conditions that justify this approximation, we notice that, if the Poynting vectors of the two electromagnetic waves reflected into each other by the grating make angles $\pm\theta$ with the propagation axis (i.e., with the longitudinal grating itself), then, in the unnormalized form, the combinations of derivatives appear in Eqs. (5) [or Eqs. (6)] as

$$ik\left[(\cos\theta)\frac{\partial U}{\partial z} + (\sin\theta)\frac{\partial U}{\partial x}\right], \quad ik\left[(\cos\theta)\frac{\partial V}{\partial z} - (\sin\theta)\frac{\partial V}{\partial x}\right] \quad (9)$$

(z is the propagation distance, which is replaced by t in the normalized equations, and $k=2\pi/\lambda$ is the wavenumber corresponding to carrier wavelength λ). As mentioned above, a typical transverse width of spatial solitons in photorefractive media is $W_\perp \sim 10-30\ \mu$m. Assuming the carrier wavelength $\simeq 1\ \mu$m, one concludes that the diffraction, represented by the second derivatives, $(1/2)\partial^2 U/\partial x^2$ and $(1/2)\partial^2 V/\partial x^2$, is negligible provided that $\theta \gtrsim 1°$.

The alternative model, based on Eqs. (6), may be related to a different setting, with a bulk photoinduced longitudinal lattice (rather than the material one, permanently written in the cladding). However, in that case CMEs [Eqs. (6)] may only be considered as providing for a phenomenological description of the setting, as a consistent derivation may lead to more complex equations; see [31]. Nevertheless, we will consider the system [Eq. (6)] too, which will help us to distinguish between more general findings and model-specific ones.

Both models conserve the total norm of the field (alias the total power, in terms of the spatial-domain transmission),

$$E = \int_{-\infty}^{+\infty} [|U(x)|^2 + |V(x)|^2]{\rm d}x. \quad (10)$$

In addition, Eqs. (5) admit the Hamiltonian representation in the ordinary form, $iU_t = \delta H/\delta U^*$, $iV_t = \delta H/\delta V^*$, where the asterisk stands for the complex conjugate, and the Hamiltonian, which is another dynamical invariant of Eqs. (5), is

$$H = \frac{1}{2}\int_{-\infty}^{+\infty} [i(UU_x^* - VV_x^*) + \ln(1 + |U|^2 + |V|^2) - 2\kappa U^* V]{\rm d}x + {\rm c.c.},$$

with c.c. standing for the complex conjugate expression. Equations (5) also conserve the total momentum,

$$P = i\int_{-\infty}^{+\infty} (UU_x^* + VV_x^*){\rm d}x. \quad (11)$$

On the other hand, a Hamiltonian representation of phenomenological equations (6), as well as their accurate

physical derivation, is not obvious; that is why the latter CME system was called "more formal" above.

To conclude the introduction of the models, we note that, if the nonlinearity is weak, the expansion of the saturable nonlinearity in all the above-mentioned CME systems, Eqs. (3)–(6), generates cubic SPM and XPM terms in the lowest approximation, and various quintic terms as first corrections to it. In this connection, it is relevant to mention that gap solitons in the coupled-mode BG equations, including self-focusing cubic and self-defocusing quintic terms, were studied in [38]. Two different types of gap solitons were identified in that work, namely, regular and "two-tiered" ones, dominated by the cubic and quintic nonlinearity, respectively. Stability regions for these soliton species are separated, similar to the above-mentioned property of the stability region for solitons in Eqs. (4). A principal difference between models with the cubic–quintic and full saturable nonlinearity is that the amplitude of soliton solutions is bounded in the former case, whereas it may be arbitrarily large in the latter one (in particular, in the models considered in this work; see below). The latter feature is explained by the fact that the saturable nonlinearity does not imply the competition between self-focusing and self-defocusing terms.

The rest of the paper is organized as follows. In Section 2, we present families of fundamental solitons (including moving and tilted ones) in the first model, based on Eqs. (5). These solutions are obtained by means of numerical methods, but the cutoff point, at which the families terminate *inside* the bandgap, and power indices that determine the divergence of the solutions near the cutoff, are found analytically. In Section 3, we report, in a more brief form, similar results for the second (phenomenological) model, which is based on Eqs. (6). In that case, the cutoff point and divergence powers are found in an analytical form, too. Dynamical results, which illustrate stability of the solitons, are presented in Section 4. That section also demonstrates the existence of two-soliton bound states in the model based on Eqs. (5). However, the bound states are unstable and transform themselves into robust breathers, with little radiation loss [Eqs. (6) do not give rise to bound states]. Results for collisions between moving (tilted) solitons are reported in Section 4, too. It is shown that the collisions, in both CME systems [Eqs. (5) and (6)], are quasi-elastic, thus being essentially different from what was found in the standard model, based on Eqs. (1), where the collisions may be strongly inelastic [39]. Section 5 concludes the paper.

2. FAMILIES OF BRAGG-GRATING SOLITONS IN THE MODEL WITH SATURABLE NONLINEARITY

A. Straight (Zero-Velocity) Solitons

We start the analysis by looking for stationary solutions of Eqs. (5) for quiescent solitons (i.e., ones with zero velocity, which correspond to zero tilt in the spatial domain), in the ordinary form,

$$\{U,V\} = \{u(x),v(x)\}\exp(-i\omega t). \tag{12}$$

The substitution of this expression in Eqs. (5) leads to a system of stationary equations. Similar to zero-velocity soliton solutions of Eqs. (1), the solutions in the present case obey a constraint compatible with the equations, $v=-u^*$, which reduces the stationary system to a single equation:

$$\omega u + i\frac{du}{dx} - \frac{u}{1+2|u|^2} - \kappa u^* = 0. \tag{13}$$

First, we report numerically obtained soliton solutions of Eq. (13), whose generic examples are displayed in Fig. 1. For comparison, the figure also includes, for the same values of parameters, well-known exact solutions of the standard CMEs [Eqs. (1)], that were found in [4,5]. Figure 1(a) presents solitons located close to the upper edge of the gap, where they are similar to their counterparts in the standard BG model (which, in this limit, is itself close to the ordinary nonlinear Schrödinger equation [40]), and Fig. 1(b) displays an example taken near the *cutoff point*, $\omega=\kappa$ [see Eq. (14)], where the newly found solitons are drastically different from the exact solutions of the standard model. In the latter case, we observe a real compo-

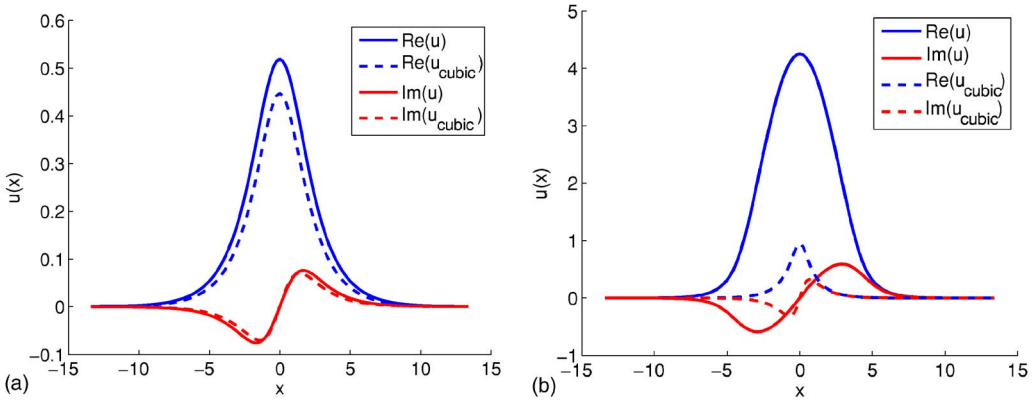

Fig. 1. (Color online) Typical examples of stable straight (zero-velocity) solitons found in the Bragg-grating model with the nonlinearity saturation. The solitons are obtained as numerical solutions of Eq. (13) with $\kappa=1$. (a) and (b) correspond to $\omega=1.8$ and 1.1, i.e., to the solitons located, respectively, close to the upper edge and center of the bandgap. Here and in Figs. 3 and 5, profiles marked by "cubic" display, for the sake of comparison, exact solutions for the gap solitons in the standard model, which is based on Eqs. (1) with the cubic nonlinearity [to make them as close as possible to Eqs. (5), we set $\sigma=1$ in Eqs. (1)]. The latter solutions were taken also for $\kappa=1$, with the substitution of $\omega\to\omega-1$, see Eq. (7).

nent $u(x)$, which is much larger than both the imaginary part of the same solution, and real and imaginary parts of the corresponding gap-soliton solution of the standard BG model with the cubic nonlinearity.

Collecting results of the numerical solution of Eq. (13) at different values of ω, it is possible to construct a family of gap-soliton solutions for given κ. As a global characteristic of the family, in Fig. 2 we have plotted (for $\kappa=1.5$) the soliton's norm, defined by Eq. (10), versus ω. A conclusion is that for all values of the coupling constant considered (we analyzed in detail the situation for $\kappa \geq 1$), the family of gap-soliton solutions to Eq. (13) fills out a stripe,

$$\kappa < \omega < 1 + \kappa, \tag{14}$$

inside the bandgap given by Eq. (8); in the remaining part of the gap, $1-\kappa<\omega<\kappa$ (which does not exist for $\kappa<1/2$), the solutions could not be found.

To explain these results, it is necessary to take into account the peculiarities of the gap-soliton solutions to Eq. (13) highlighted above, in connection to Fig. 1(a). Indeed, approaching the cutoff point, $\omega=\kappa$, where the solutions cease to exist, we observe broad solitons with a large real part of $u(x)$, and bounded $\mathrm{Im}[u(x)]$. Analyzing Eq. (13), one easily concludes that, at $\omega-\kappa\to 0$, the amplitude of $\mathrm{Re}[u(x)]$, A, diverges simultaneously with the soliton's width, W, as

$$A \sim W \sim (\omega - \kappa)^{-1/2}, \tag{15}$$

while the amplitude of $\mathrm{Im}[u(x)]$ remains finite (the saturable nonlinearity, unlike the above-mentioned cubic–quintic one [38], admits solitons with an arbitrarily large amplitude). Simultaneously, the soliton is much broader than its counterpart in the standard model. This entails an estimate for the respective divergence of the soliton norm,

$$E \sim A^2 W \sim (\omega - \kappa)^{-3/2}, \tag{16}$$

which agrees with the numerical results shown in Fig. 2.

As mentioned above, the existence region for the gap solitons given by Eq. (14) actually covers the entire bandgap [see Eq. (8)], at small values of the coupling constant, $\kappa<0.5$. While we did not study this case in detail, assuming that the systems with relatively strong coupling, $\kappa \geq 1$, are of major interest, we assume that, for small κ, the gap-soliton family is similar to that in the standard model based on Eqs. (1).

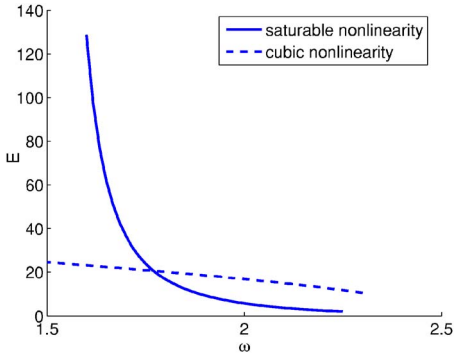

Fig. 2. (Color online) Norm of the soliton, defined as per Eq. (10), versus ω for the family of numerically found straight (zero-velocity) soliton solutions to Eq. (13), with $\kappa=1.5$. The family exists in interval $1.5<\omega<2.5$, which corresponds to Eq. (14). For $\omega-1.5\to 0$, the norm diverges, as the amplitude of the real part of the solution and its width tend to become infinitely large; see Fig. 1(b). For the sake of comparison, a curve showing the norm of the family of exact solitons in the standard model, based on Eqs. (1) with $\sigma=1$, *multiplied by 10* (otherwise, it would be almost invisible) is included too.

B. Tilted (Moving) Solitons

Solutions to Eqs. (5) for solitons moving at velocity c (recall they appertain to tilted beams, in the spatial-domain interpretation of the model) were looked for as $\{U,V\}=\{u(x-ct),v(x-ct)\}\exp(-i\omega t)$. The substitution of this in Eqs. (5) leads to a system of stationary equations,

$$\omega u + (1-c)i\frac{du}{d\xi} - \frac{u}{1+|u|^2+|v|^2} + \kappa v = 0,$$

$$\omega v - (1+c)i\frac{dv}{d\xi} - \frac{v}{1+|v|^2+|u|^2} + \kappa u = 0, \tag{17}$$

where $\xi \equiv x-ct$. Unlike the case of $c=0$, these equations do not admit reduction $v=-u^*$, hence Eqs. (17) cannot be reduced to a single equation, such as Eq. (13).

Because the linearization of Eqs. (17) is identical to that of standard CMEs [Eqs. (1)], the interval of the ve-

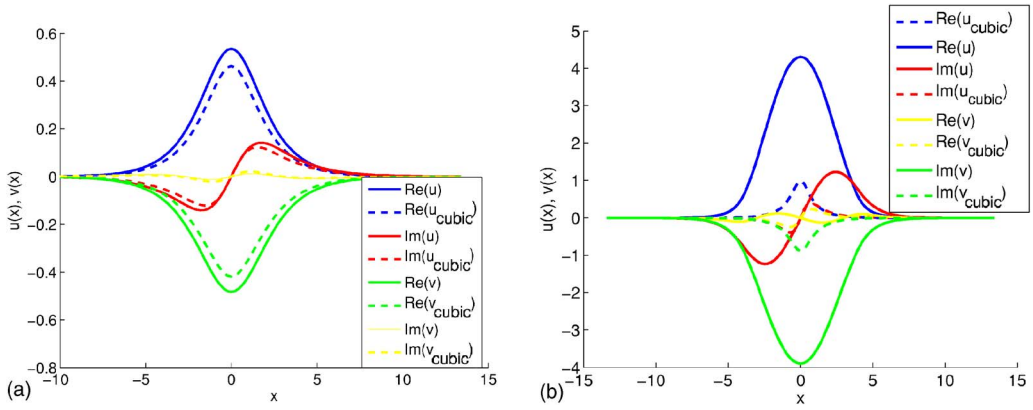

Fig. 3. (Color online) Examples of stable tilted (moving) solitons in the BG model with the saturable nonlinearity, for $\kappa=1$, $c=0.1$, and $\omega=1.8$ (a) and $\omega=1.1$ (b), i.e., respectively, close to the upper edge and center of the bandgap, cf. Fig. 1. For comparison, exact solutions for the moving solitons found, at the same parameters, in the standard model based on Eqs. (1), with $\sigma=1$, are included too.

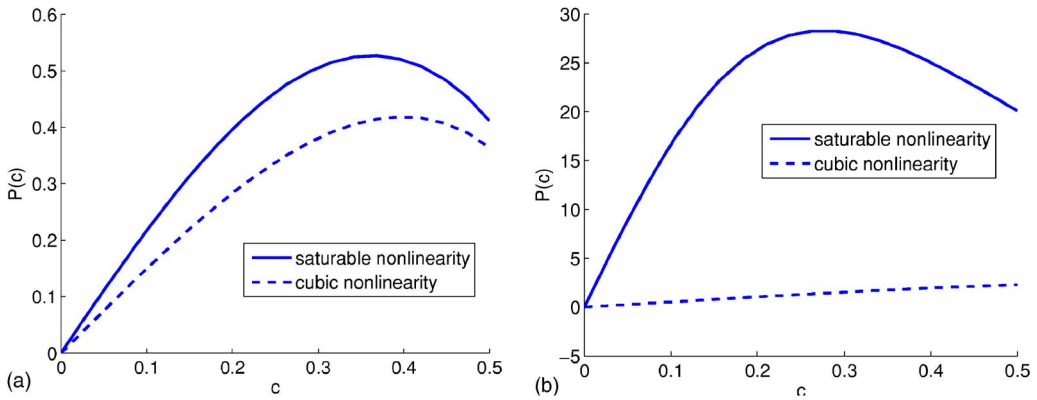

Fig. 4. (Color online) Momentum of the moving (tilted) solitons, found as per Eq. (11), plotted versus their velocity, for $\kappa=1$. The intrinsic frequency of the solitons is fixed at (a) $\omega=1.8$ and (b) $\omega=1.1$. The $P(c)$ dependences for exact solitons in the standard model, based on Eqs. (1), with $\sigma=1$, are included for the comparison.

locities in which the solitons may exist in the present model is the same as in the standard one, i.e., $-1<c<+1$ (it is found as an interval of values of c for which the linearization of the equations in the moving coordinates still yields a finite bandgap).

Shapes of the moving solitons were found from a numerical solution of Eqs. (17). Typical examples of moving solitons and comparison with their counterparts in the standard BG model are given in Fig. 3.

As well as the straight (zero-velocity) solutions, their counterparts for the tilted (moving) solitons fill out only a part of the available bandgap. Indeed, a straightforward analysis shows that soliton solutions to Eqs. (17) can only be found for $\omega>\kappa$ (i.e., the cutoff point, $\omega=\kappa$, does not depend on the velocity, as corroborated by numerical solutions for the moving solitons), and estimates [Eqs. (15) and (16)] that were derived above for the straight (zero-velocity) solitons, remain valid for the tilted (moving) ones as well. Note that the soliton existence region, $\omega>\kappa$, covers the entire bandgap in the comoving reference frame at $\kappa<1/(1+\sqrt{1-c^2})$; cf. the above-mentioned condition, $\kappa<1/2$, for the straight (zero-velocity) solitons.

For given values of ω, the family of moving solitons is characterized by the dependence of the momentum on the velocity, $P(c)$, with P defined by Eq. (11). Typical examples of this dependence are displayed in Fig. 4.

3. SOLITON FAMILIES IN THE MODEL WITH THE SATURATION OF THE NONLINEARITY AND COUPLING

Proceeding to the analysis of solitons in the phenomenological model based on Eqs. (6), which includes the saturation of the intermode coupling, we start with the straight (zero-velocity) solutions, in the form of Eq. (12). Substituting it in Eqs. (6) and using the above-mentioned constraint, $v=-u^*$, we reduce the stationary equations to a single one [cf. Eq. (13)],

$$\omega u + i\frac{du}{dx} - \frac{u+\kappa u^*}{1+2|u|^2} = 0. \tag{18}$$

The analysis of Eq. (18) readily demonstrates that, in this model, the cutoff point is $\omega=0$ (if it belongs to the bandgap [Eq. (8)], i.e., if $\kappa\geq 1$), with the solitons filling the region of

$$0<\omega<1+\kappa. \tag{19}$$

Note that this region is broader than its counterpart in the previously considered model, which was given by Eq. (14). In the limit of $\omega\to+0$, analysis of Eq. (18) predicts the following divergence scalings for the soliton's amplitude, width, and norm [cf. Eqs. (15) and (16)]:

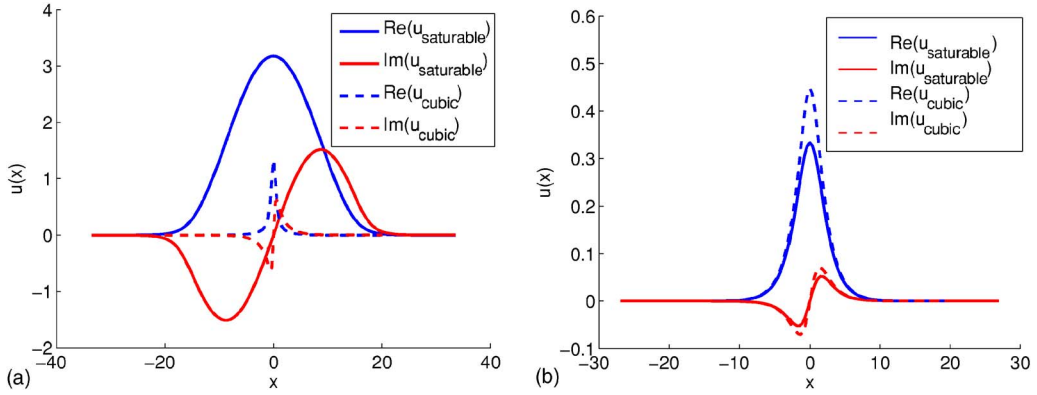

Fig. 5. (Color online) Examples of stable straight (zero-velocity) solitons found in the BG model with the coupling saturation, based on Eqs. (6) with $\kappa=1$: (a) $\omega=0.18$; (b) $\omega=1.8$. For comparison, solitons in the standard BG model, based on Eqs. (1) and found at the corresponding values of parameters (in particular, $\sigma=1$), are shown too.

$$A \sim \omega^{-1/2}, \quad W \sim \omega^{-1}, \quad E \sim \omega^{-2}. \tag{20}$$

Typical examples of solitons produced by numerical solution of Eq. (18) are displayed in Fig. 5 [together with their counterparts found in the standard model based on Eqs. (1)], and the $E(\omega)$ dependence for the family is shown in Fig. 6. Solutions for moving (tilted) solitons have also been found in this model, in the entire region of velocities where they are expected to exist, $-1 < c < +1$. Examples of the moving solitons are given in Fig. 7.

4. DYNAMICAL PROBLEMS: STABILITY OF THE SOLITONS, BOUND STATES, AND COLLISIONS

A. Stability Analysis

The next step in the study of the present models is to consider stability of the solitons. To this end, we note, first of all, that the $E(\omega)$ dependences displayed in Figs. 2 and 6 satisfy the Vakhitov–Kolokolov (VK) criterion, $dE/d\omega < 0$, according to which solitons cannot be unstable against perturbation eigenmodes with purely real instability growth rates [41]. However, the VK criterion ignores perturbations with complex growth rates. In particular, it is well known that, while all soliton solutions in the BG model with the cubic nonlinearity, based on Eqs. (1), meet the condition of $dE/d\omega < 0$, only half of them are truly stable [6–8].

To analyze the stability of zero-velocity solutions in the model with the saturable nonlinearity in a consistent way, we employ the linearization of Eqs. (5). To this end, we take a perturbed solution as

$$\begin{Bmatrix} U(x,t) \\ V(x,t) \end{Bmatrix} = \left[\begin{Bmatrix} u_0(x) \\ v_0(x) \end{Bmatrix} + \begin{Bmatrix} u_1(x) \\ v_1(x) \end{Bmatrix} e^{i\lambda t} \right] e^{-i\omega t},$$

where $u_0(x)$ and $v_0(x)$ are components of the unperturbed solution, and functions $u_1(x)$ and $v_1(x)$ constitute an eigenmode of small perturbations with a (generally speaking, complex) instability growth rate λ. Upon the substitution of this in Eqs. (5) and linearization, we arrive at coupled equations for the components of the perturbation eigenmode (if the unperturbed soliton is straight, i.e., it has zero velocity),

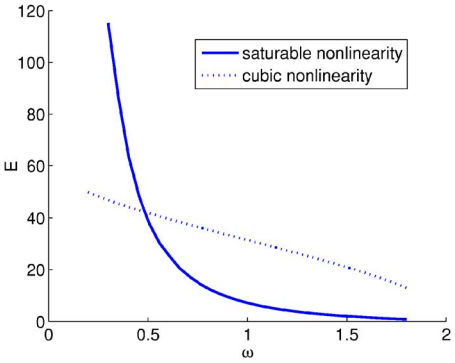

Fig. 6. (Color online) Norm of the soliton defined as per Eq. (10), is plotted versus ω for the family of numerically found straight (zero-velocity-) soliton solutions of Eq. (18), with $\kappa = 1$. The family exists in the interval [Eq. (19)], which, in the present case, is $0 < \omega < 2$, coinciding with the entire bandgap [Eq. (8)] (for $\kappa > 1$, the existence interval is smaller than the bandgap; see text). For $\omega \to 0$, the norm, amplitude and width of the soliton diverge in accordance with analytical predictions [Eq. (20)]. For comparison, a curve showing the norm of the family of exact solitons in the standard model, based on Eqs. (1) with $\sigma = 1$ and $\kappa = 1$, multiplied by 10 (to make it visible), is included too, cf. Fig. 2.

$$\left(\omega + i\frac{d}{dx}\right)u_1 - \frac{u_1}{1 + |u_0|^2 + |v_0|^2} + \frac{(u_1 u_0^* + u_0 u_1^*) + v_1 v_0^* + v_0 v_1^*}{(1 + |u_0|^2 + |v_0|^2)^2} u_0 + \kappa v_1 = \lambda u_1,$$

$$\left(\omega - i\frac{d}{dx}\right)v_1 - \frac{v_1}{1 + |v_0|^2 + |u_0|^2} + \frac{(v_1 v_0^* + v_0 v_1^*) + u_1 u_0^* + u_0 u_1^*}{(1 + |v_0|^2 + |u_0|^2)^2} v_0 + \kappa u_1 = \lambda v_1.$$

The eigenvalue problem based on these equations (complex conjugates of the equations were used to close the linear system) was solved numerically. The obtained results show that, within the numerical accuracy available, the instability growth rate for the straight (zero-velocity) solitons is zero, in the entire region where they exist. We stress that this result was obtained for the model with $\kappa \geq 1$, when the existence region, given by Eq. (14), occupies

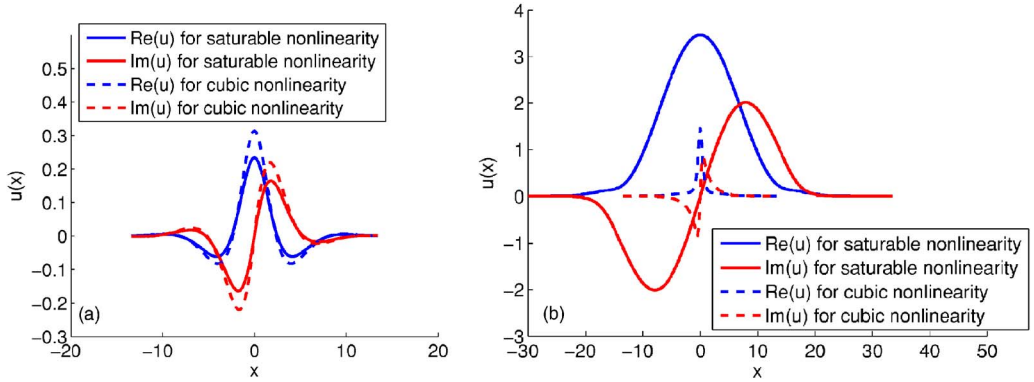

Fig. 7. (Color online) Examples of stable moving (tilted) solitons in the model with the saturation of the nonlinearity, for $\kappa = 1$: (a) $c = 0.5$, $\omega = 1.8$ and (b) $c = 0.2$, $\omega = 0.18$, i.e., near the upper and lower edge of the bandgap, respectively; cf. Fig. 3. For comparison, included are also exact solutions for the moving solitons (at the corresponding values of the parameters) in the standard model based on Eqs. (1), with $\sigma = 1$.

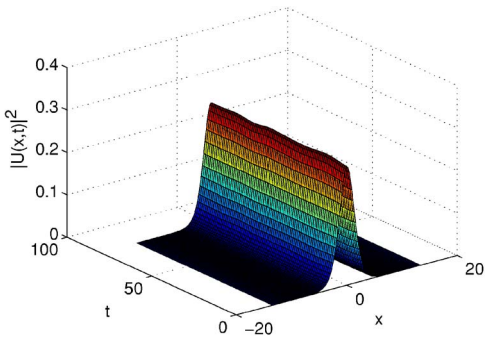

Fig. 8. (Color online) Evolution of a perturbed straight (zero-velocity) soliton in the model based on Eqs. (5), for $\kappa=1$ and $\omega=1.8$, i.e., when the unperturbed soliton is the same as in Fig. 1. In this figure and in other figures that present results of direct simulations (see below) only the U component is displayed, as the evolution of its V counterpart seems quite similar, in all cases.

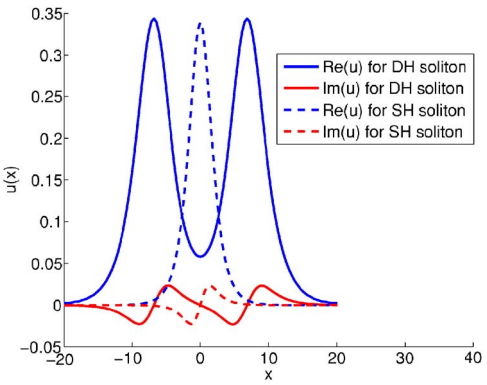

Fig. 10. (Color online) Typical example of a DH stationary pattern found from Eq. (13) at $\omega=3.4$ and $\kappa=2.5$. For comparison, a fundamental (SH) soliton, found at the same values of parameters, is shown too.

less than a half of the entire bandgap, see Eq. (8). On the other hand, in the standard BG model, with the cubic nonlinearity, an approximate analytical consideration [6] and accurate numerical analysis [7,8] of Eqs. (1) reveal that only the solitons from the upper-half bandgap, $0 \leq \omega < \kappa$, are stable, while the remaining half, $-\kappa < \omega < 0$, is occupied by unstable solitons (as mentioned above). A possible explanation to the complete stability of the gap-soliton family in the present model is that a part of the bandgap where unstable solitons could be found is actually empty.

The stability of the solitons has also been verified by direct simulations of the evolution of perturbed solitons in the framework of the underlying Eqs. (5). A typical example attesting to the stability of the solitons, with the initial perturbation amplitude at a 2% level, is shown in Fig. 8.

The stability of tilted (moving) solitons has also been analyzed, by computing eigenvalues determined by the linearization of Eqs. (5) in the reference frame moving along with the unperturbed soliton and also by means of direct simulations of perturbed solitons. It has been concluded that, as well as their zero-velocity (straight) counterparts, the moving (tilted) solitons do not give rise to unstable eigenvalues, within the framework of the available numerical accuracy. Direct simulations of Eqs. (5) confirm the stability of the moving solitons. Examples, obtained by adding a perturbation to the moving solitons at the amplitude level of 2%, are displayed in Fig. 9; cf. Fig. 8.

A similar analysis has been performed for the solitons in the model based on Eqs. (6), which includes the saturation of the linear coupling. The results are similar too, demonstrating the stability of the solitons, as determined by the computation of the eigenvalues and verified in direct simulations. Moving solitons in this model are also stable.

B. Bound States of Solitons

Some other models based on the linear coupling between waves induced by the Bragg reflection feature double-hump (DH) stationary solitons, in addition to the fundamental single-hump (SH) ones. Examples are three-wave [14] and four-wave [42,43] systems with quadratic nonlinearity. Similar states were also found in a model with saturable nonlinearity, but without the BG-induced coupling [44].

Besides the fundamental solitons reported above, numerical solution of the stationary equation, which determines zero-velocity solitons in the model with the nonlinearity saturation, Eq. (13), gives rise to DH solitons in this model, too; they may be realized as in-phase bound states of the fundamental solitons; see an example in Fig. 10. This result, by itself, is nontrivial, as no such states are known in the standard BG model based on Eqs. (1),

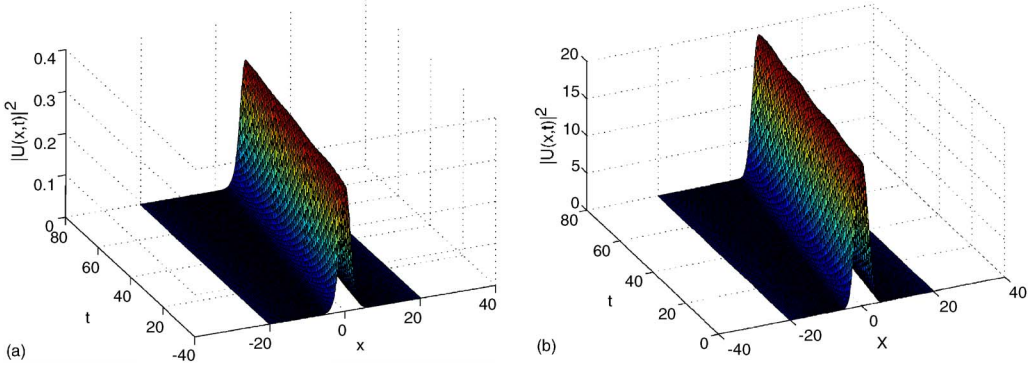

Fig. 9. (Color online) Evolution of the tilted (moving) solitons from Figs. 3(a) and 3(b), to which a 2% amplitude perturbation was added.

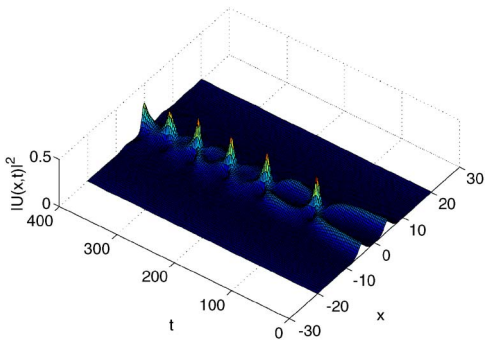

Fig. 11. (Color online) Transformation of the unstable bound state of two in-phase solitons into a breather, at $\kappa=2.5$ and $\omega=3.4$ (the initial bound state is the same as in Fig. 10).

and numerical solution of the other coupled-mode system introduced above, viz., the one based on Eqs. (6), have not revealed any bound states either. However, direct simulations of Eqs. (5), with the DH solitons taken as initial conditions, demonstrate that they are unstable. A typical example displayed in Fig. 11 shows that the instability initiates repeated collisions of two solitons that originally form the bound state. Eventually, they merge into quite a robust breather, that features indefinitely long quasi-regular vibrations. The transformation of the unstable bound state into the breather gives rise to little radiation loss: in the case shown in Fig. 11, the relative difference of the norm [Eq. (10)] between the initial and final localized states is 5%.

Barring numerical problems with solutions for very broad solitons, a conclusion is that the bound states of two fundamental solitons, which transform themselves into breathers due to the instability, can be found at all values of ω at which the fundamental solitons themselves exist. It is also relevant to mention that no stable or unstable bound states formed by three (or more) solitons have been found in Eqs. (5).

C. Collisions between Moving Solitons

The existence of stable moving solitons suggests a possibility to simulate collisions between them. In the standard BG model with the cubic nonlinearity, based on Eqs. (1) with $\sigma=0.5$, collisions were systematically investigated in [39]. It was found that identical solitons moving with velocities $\pm c$ collide quasi-elastically (passing through each other, with some loss and excitation of intrinsic oscillations) if c exceeds 0.2; at $c<0.2$, the slowly moving solitons could merge into a single pulse; see an example of the latter outcome of the collision in Fig. 12(a).

We have performed systematic simulations of the collisions in the two models introduced in this work, i.e., ones based on Eqs. (5) and (6). In either system, the collisions always appear to be quasi-elastic, i.e., the solitons separate after the collision, featuring some intrinsic perturbations. A typical example of the quasi-elastic collision of slow solitons, with velocities $c=\pm 0.1$, is shown in Fig. 12(b).

5. CONCLUSION

In this work, we have introduced two coupled-mode systems describing the copropagation of two waves coupled by the resonant Bragg reflection in a medium with saturable nonlinearity. The main model, based on coupled-mode equations in the form of Eqs. (5), combines the rational nonlinearity and ordinary (linear) coupling. It may be realized in the spatial domain, considering a planar waveguide made of a photorefractive material, with the longitudinal diffraction lattice written in its cladding, which is made of an ordinary optical material. We have demonstrated analytically and confirmed by numerical results that, unless the coupling is too weak, there is a cutoff point ($\omega=\kappa$) inside the system's bandgap, with gap solitons existing to the right of it. The powers that determine the divergence of the soliton's amplitude, width and norm close to the cutoff point were predicted in the analytical form and corroborated by numerical computations. The computation of the stability eigenvalues for small perturbations and direct simulations demonstrate that the solitons existing between the cutoff point and the upper edge of the bandgap are stable, which pertains to straight (zero-velocity) and tilted (moving) solitons alike. In-phase bound states of two fundamental solitons have been found too, but they are unstable, and eventually merge into robust breathers, with little radiation loss at the transient stage.

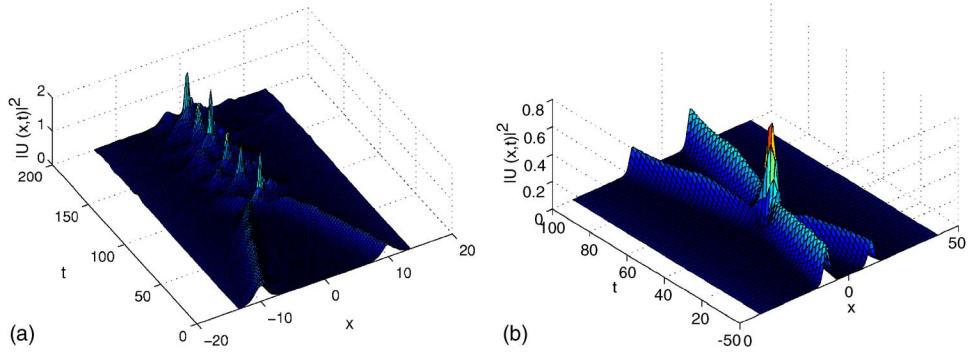

Fig. 12. (Color online) Examples of collisions between identical solitons moving at velocities $\pm c$: (a) the inelastic collision at $c=0.1$, produced by simulations of the standard BG model, based on Eqs. (1) with $\sigma=0.5$; (b) quasi-elastic collision at the same velocities, $c=0.1$, revealed by simulations of Eqs. (5). In both cases, the equations were taken with $\kappa=1$, and the colliding solitons had intrinsic frequencies (a) $\omega=0.6675$ and (b) $\omega=1.8$.

The second model introduced in this work, based on Eqs. (6), is a phenomenological one. It assumes a bulk photoinduced grating, therefore this model features the saturation of the intermode coupling, in addition to the nonlinearity saturation. In that case, the cutoff point, $\omega = 0$, and the law of divergence of the soliton solutions close to it were also found analytically and confirmed numerically. The solitons are stable in this model too, while it does not give rise to two-soliton bound states, stable or unstable ones.

Collisions between solitons in the present models were explored by means of direct simulations. It was concluded that, on the contrary to the standard Bragg-grating model, the collisions are always quasi-elastic in both systems of the CMEs introduced in this work.

ACKNOWLEDGMENTS

I. M. Merhasin and K. Nakkeeran appreciate financial support from (through project G-YE30) and hospitality of the Department of Electronic and Information Engineering at The Hong Kong Polytechnic University. B. A. Malomed acknowledges hospitality of the Department of Mechanical Engineering at the University of Hong Kong. The work of I. M. Merhasin and B. A. Malomed is supported, in part, by the Israel Science Foundation through Center-of-Excellence grant 8006/03, and by the German-Israel Foundation through grant 1-800-149.7/2005. K. W. Chow and K. Nakkeeran acknowledge the Royal Society for support in the form of an International Joint Project Grant. K. W. Chow and K. Nakkeeran are grateful to John Watson for his valuable support of this research collaboration. K. Nakkeeran also acknowledges the Nuffield Foundation for financial support through the Newly Appointed Lecturer Award and financial support from The Hong Kong Polytechnic University.

REFERENCES

1. R. Kashyap, *Fiber Bragg Gratings* (Academic, 1999).
2. Y. S. Kivshar and G. P. Agrawal, *Optical Solitons* (Academic, 2003).
3. C. M. de Sterke and J. E. Sipe, "Gap solitons," in *Progress in Optics*, E. Wolf, ed. (North-Holland, 1994), Vol. XXXIII, Chap. III, pp. 203–260.
4. A. B. Aceves and S. Wabnitz, "Self-induced transparency solitons in nonlinear refractive periodic media," Phys. Lett. A **141**, 37–42 (1989).
5. D. N. Christodoulides and R. I. Joseph, "Slow Bragg solitons in nonlinear periodic structure," Phys. Rev. Lett. **62**, 1746–1749 (1989).
6. B. A. Malomed and R. S. Tasgal, "Vibration modes of a gap soliton in a nonlinear optical medium," Phys. Rev. E **49**, 5787–5796 (1994).
7. I. V. Barashenkov, D. E. Pelinovsky, and E. V. Zemlyanaya, "Vibrations and oscillatory instabilities of gap solitons," Phys. Rev. Lett. **80**, 5117–5120 (1998).
8. A. De Rossi, C. Conti, and S. Trillo, "Stability, multistability, and wobbling of optical gap solitons," Phys. Rev. Lett. **81**, 85–88 (1998).
9. B. J. Eggleton, R. E. Slusher, C. M. de Sterke, P. A. Krug, and J. E. Sipe, "Bragg grating solitons," Phys. Rev. Lett. **76**, 1627–1630 (1996).
10. B. J. Eggleton, C. M. De Sterke, and R. E. Slusher, "Bragg solitons in the nonlinear Schrödinger limit: experiment and theory," J. Opt. Soc. Am. B **16**, 587–599 (1999).
11. J. Feng, "Alternative scheme for studying gap solitons in an infinite periodic Kerr medium," Opt. Lett. **18**, 1302–1304 (1993).
12. R. F. Nabiev, P. Yeh, and D. Botez, "Spatial gap solitons in periodic nonlinear structures," Opt. Lett. **18**, 1612–1614 (1993).
13. Yu. S. Kivshar, "Gap solitons due to cascading," Phys. Rev. E **51**, 1613—1615 (1995).
14. W. C. K. Mak, B. A. Malomed, and P. L. Chu, "Three-wave gap solitons in waveguides with quadratic nonlinearity," Phys. Rev. E **58**, 6708–6722 (1998).
15. A. A. Sukhorukov and Yu. S. Kivshar, "Discrete gap solitons in modulated waveguide arrays," Opt. Lett. **27**, 2112–2114 (2002).
16. P. G. Kevrekidis, B. A. Malomed, and Z. Musslimani, "Discrete gap solitons in a diffraction-managed waveguide array," Eur. Phys. J. D **23**, 421–236 (2003).
17. D. Mandelik, H. S. Eisenberg, Y. Silberberg, R. Morandotti, and J. S. Aitchison, "Band-gap structure of waveguide arrays and excitation of Floquet–Bloch solitons," Phys. Rev. Lett. **90**, 053902 (2003).
18. D. Mandelik, R. Morandotti, J. S. Aitchison, and Y. Silberberg, "Gap solitons in waveguide arrays," Phys. Rev. Lett. **92**, 093904 (2004).
19. R. Morandotti, D. Mandelik, Y. Silberberg, J. S. Aitchison, M. Sorel, D. N. Christodoulides, A. A. Sukhorukov, and Y. S. Kivshar, "Observation of discrete gap solitons in binary waveguide arrays," Opt. Lett. **29**, 2890–2892 (2004).
20. F. Chen, M. Stepić, C. E. Rüter, D. Runde, D. Kip, V. Shandarov, O. Manela, and M. Segev, "Discrete diffraction and spatial gap solitons in photovoltaic $LiNbO_3$ waveguide arrays," Opt. Express **13**, 4314–4324 (2005).
21. J. W. Fleischer, T. Carmon, M. Segev, N. K. Efremidis, and D. N. Christodoulides, "Observation of discrete solitons in optically induced real time waveguide arrays," Phys. Rev. Lett. **90**, 023902 (2003).
22. D. Neshev, A. A. Sukhorukov, B. Hanna, W. Krolikowski, and Yu. S. Kivshar, "Controlled generation and steering of spatial gap solitons," Phys. Rev. Lett. **93**, 083905 (2004).
23. W. Fleischer, M. Segev, N. K. Efremidis, and D. N. Christodoulides, "Observation of two-dimensional discrete solitons in optically induced nonlinear photonic lattices," Nature **422**, 147–150 (2003).
24. N. K. Efremidis, S. Sears, D. N. Christodoulides, J. W. Fleischer, and M. Segev, "Discrete solitons in photorefractive optically induced photonic lattices," Phys. Rev. E **66**, 046602 (2002).
25. N. K. Efremidis, J. Hudock, D. N. Christodoulides, J. W. Fleischer, O. Cohen, and M. Segev, "Two-dimensional optical lattice solitons," Phys. Rev. Lett. **91**, 213906 (2003).
26. G. Bartal, O. Cohen, T. Schwartz, O. Manela, B. Freedman, M. Segev, H. Buljan, and N. K. Efremidis, "Spatial photonics in nonlinear waveguide arrays," Opt. Express **13**, 1780–1796 (2005).
27. X. Wang, Z. Chen, and P. G. Kevrekidis, "Observation of discrete solitons and soliton rotation in optically induced periodic ring lattices," Phys. Rev. Lett. **96**, 083904 (2006).
28. B. B. Baizakov, B. A. Malomed, and M. Salerno, "Matter-wave solitons in radially periodic potentials," Phys. Rev. A **70**, 053613 (2004).
29. Y. V. Kartashov, V. A. Vysloukh, and L. Torner, "Rotary solitons in Bessel optical lattices," Phys. Rev. Lett. **93**, 093904 (2004).
30. Y. V. Kartashov, V. A. Vysloukh, and L. Torner, "Stable ring-profile vortex solitons in Bessel optical lattices," Phys. Rev. Lett. **94**, 043902 (2005).
31. B. A. Malomed, T. Mayteevarunyoo, E. A. Ostrovskaya, and Y. S. Kivshar, "Coupled-mode theory for spatial gap solitons in optically induced lattices," Phys. Rev. E **71**, 056616 (2005).
32. O. Cohen, T. Carmon, M. Segev, and S. Odoulov, "Holographic solitons," Opt. Lett. **27**, 2031–2033 (2002).
33. M. Belić, Ph. Jander, A. Strinic, A. Desyatnikov, and C. Denz, "Self-trapped bidirectional waveguides in a saturable photorefractive medium," Phys. Rev. E **68**, R025601 (2003).

34. K. Motzek, Ph. Jander, A. Desyatnikov, M. Belić, C. Denz, and F. Kaiser, "Dynamic counterpropagating vector solitons in saturable self-focusing media," Phys. Rev. E **68**, 066611 (2003).
35. M. Segev, B. Crosignani, A. Yariv, and B. Fischer, "Spatial solitons in photorefractive media," Phys. Rev. Lett. **68**, 923–926 (1992).
36. G. C. Duree, J. L. Shultz, G. J. Salamo, M. Segev, A. Yariv, B. Crosignani, P. Di Porto, E. J. Sharp, and R. R. Neurgaonkar, "Observation of self-trapping of an optical beam due to the photorefractive effect," Phys. Rev. Lett. **71**, 533–536 (1993).
37. S. Lan, M. Shih, and M. Segev, "Self-trapping of one-dimensional and two-dimensional optical beams and induced waveguides in photorefractive $KNbO_3$," Opt. Lett. **22**, 1467–1469 (1997).
38. J. Atai and B. A. Malomed, "Families of Bragg-grating solitons in a cubic–quintic medium," Phys. Lett. A **155**, 247–252 (2001).
39. W. C. K. Mak, B. A. Malomed, and P. L. Chu, "Formation of a standing-light pulse through collision of gap solitons," Phys. Rev. E **68**, 026609 (2003).
40. N. M. Litchinitser, B. J. Eggleton, and D. B. Patterson, "Fiber Bragg gratings for dispersion compensation in transmission: theoretical model and design criteria for nearly ideal pulse recompression," J. Lightwave Technol. **15**, 1303–1313 (1997).
41. M. G. Vakhitov and A. A. Kolokolov, "Stationary solutions of the wave equation in a medium with nonlinearity saturation," Sov. J. Radiophys. Quantum Electr. **16**, 783–789 (1973) [Izv. Vuz. Radiofiz. **16**, 1020–1028 (1973)].
42. T. Peschel, U. Peschel, F. Lederer, and B. A. Malomed, "Solitary waves in Bragg gratings with a quadratic nonlinearity," Phys. Rev. E **55**, 4730–4739 (1997).
43. Y. Leitner and B. A. Malomed, "Stability of double-peaked solitons in Bragg gratings with the quadratic nonlinearity," Phys. Rev. E **71**, 057601 (2005).
44. E. A. Ostrovskaya, Y. S. Kivshar, D. V. Skryabin, and W. J. Firth, "Stability of multihump optical solitons," Phys. Rev. Lett. **83**, 296–299 (1999).